THE JOURNAL OF PHYSICAL CHEMISTRY C

Article

pubs.acs.org/JPCC

The Structure, Energy, Confinement, and Enhancement of Hot Spots between Two Nanoparticles

Eduardo M. Perassi and Eduardo A. Coronado*

INFIQC, CLCM, Department de Fisicoquímica, Facultad de Ciencias Químicas, Universidad Nacional de Córdoba, Córdoba (5000), Argentina

ABSTRACT: Hot spots (HSs) between two nanoparticles (NPs) can be considered the canonical example of plasmonic coupling effects and are able to achieve huge enhancements of signals from molecules in fluorescence and Raman spectroscopy. In this work, it is found that these HSs between two NPs can be modeled as a superposition of sub-HSs that are located on the surface of each NP of the pair, a fact that can be important to describe plasmon coupling effects. The analyzed HSs are almost fully characterized by means of their energy, degree of localization, and mean enhancement, quantities that are able to give a measure of their performance. It is demonstrated that the interplay between the energy and degree of localization is what actually determines the enhancement in a general way, that is, HSs with similar energy could have a large/small enhancement depending on their degree of localization.

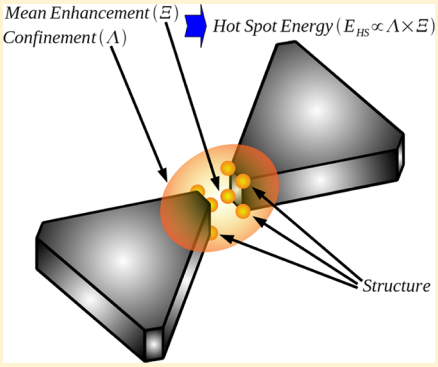

INTRODUCTION

Metallic nanoparticles (NPs) and NP aggregates have remarkable optical properties related to collective electronic excitations that are also called localized surface plasmon resonances (SPRs). These SPRs are the result of the interaction among metallic NPs and electromagnetic waves with particular wavelengths and polarizations. Among these remarkable optical properties, large electromagnetic field enhancements (Γ) around the NPs stand out by their applications. Many studies have demonstrated that Γ between two spherical NPs can be orders of magnitude higher than the values of Γ around a single spherical NP during a plasmon resonance.[1−5]

These high values of Γ between two NPs have huge impact on many different fields, specially a direct application of them can be found in all the enhanced spectroscopies like SERS (surface-enhanced Raman spectroscopy),[6−12] SM-SERS (single molecule surface-enhanced Raman spectroscopy),[13−19] TERS (tip-enhanced Raman spectroscopy),[20−29] and SEF (surface enhancement fluorescence).[30−33] In these spectroscopies, such spatial regions with high values of Γ, usually called hot spots (HSs), allow the ultrasensitive detection of molecules.

Another field of great interest is the detection of chemical and biological agents that play a crucial role in medical diagnosis, forensic, and environmental sciences. Recently, the detection of proteins, lysozyme and cytochrome, as well as live bacterial cells in aqueous solutions, have reached high values of sensitivity by taking advantage of strong Γ values within HSs among NPs.[34]

In addition, these enhanced fields are also relevant in other applications such as nanolithography,[35−38] tips for SNOM (scanning near-field optical microscopy)[39,40] and FESOM (field-enhanced scanning optical microscopy),[3] biosensors,[41−44] chemical sensors,[45] and so forth.

Developing rigorous and accurate theoretical methods for a quantitative assessment of the magnitude and confinement of Γ within HSs between two NPs is of direct interest for understanding the plasmonic coupling effects and therefore the results of experiments, as well as to improve the above-mentioned techniques. In order to study HSs around single NPs, the concept of variation of the trapped volume (VTV) has been introduced and applied to HSs on typical shapes.[46] In that work, after applying this concept to HSs on single NPs, an answer to the question of how to determine the enhancement within a finite volume element (that could be the volume of a molecule or quantum dot located inside an HS) has been given. In addition, two new quantities to measure the degree of localization and enhancement of an HS have been introduced. This VTV analysis itself demonstrated to be a procedure to analyze the convergence of electrodynamic simulations of Γ distributions around NPs in three-dimensional (3D) space.

In the present work, the concept of VTV is used to analyze HSs that are generated between the NPs of three quite different dimers: a dimer of Ag spheres, a dimer of Ag-truncated triangular prisms, and a dimer of Au irregular NPs. The choice of the first two canonical dimer structures is because they have been extensively studied both theoretically and experimentally.[47−51] The specific selection of the last nanostructure is to show the capabilities of the VTV approach to analyze interactions between NPs with more realistic shapes which are usually found in experiments.[52,53]

The performed analysis in this work indicates that the HSs between NPs can be considered as a superposition of sub-HSs

Received: September 5, 2012
Revised: March 22, 2013
Published: March 25, 2013

that are located on the surface of each NP of the dimer. Applying the VTV analysis, a new quantity that is denoted as HS energy (E_{HS}) is introduced. This E_{HS} is directly obtained from the VTV analysis by determining two intrinsic quantities of an HS, that is, the degree of localization (Λ) and the mean enhancement (Ξ). These three quantities of an HS, that is, mean enhancement, degree of localization, and energy, allow comparisons among HSs that are generated in different nanostructures because they give a full quantitative characterization of an HS.

STUDIED SYSTEM AND THEORETICAL METHODS

The dimensions and configuration of two of the nanostructures that are used for the analysis correspond to NP dimers that has been studied in a previous work by Hao and Schatz.[4] The first studied nanostructure, the dimer of spheres, is constituted by two Ag spheres that are separated by 2 nm and are 36 nm in diameter (Figure 1a). The second nanostructure correspond to

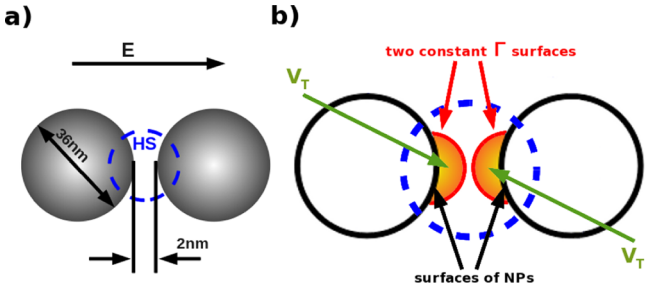

Figure 1. (a) Scheme of the studied sphere dimer. The dimensions, incident polarization, and location of the studied HS (dashed blue circle) are indicated. (b) Scheme of the two sub-HSs (yellow-orange) that are located on each NP surface (black circles).

two Ag triangular prisms that are positioned on a common plane with a common perpendicular bisector with corresponding tips directed toward each other and separated by 2 nm. Figure 2a shows that the prisms are 12 nm thick, 60 nm in edge

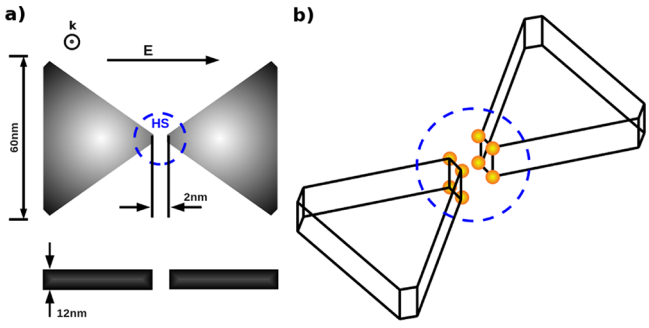

Figure 2. (a) Scheme of the studied truncated triangular prism dimer. The dimensions, incident polarization, and location of the studied HS (dashed blue circle) are indicated. (b) Scheme of the eight sub-HSs (yellow-orange) that are located on the vertices of the truncated tips of the prisms.

length, and 2 nm along the 60 nm edges have been removed from each tip. The surrounding media of these two dimers is water as it is a very frequent situation of experiments.

The extinction spectrum of the sphere dimer (not shown in this work) present a strong peak[4] at λ = 520 nm and a shoulder peak[4] at λ = 430 nm for the incident polarization and wave propagation direction that are indicated in Figure 1a. These peaks at λ = 520 nm and λ = 430 nm are denoted with the term dipole and quadrupole resonance because a expansion in spherical harmonic of the polarization about the midpoint of the spheres would be predominantly dipole and quadrupole in character, respectively. In the case of the truncated triangular prisms dimer, the extinction spectrum (not shown in this work) shows a dipole resonance[4] at λ = 932 nm and a quadrupole resonance[4] at λ = 550 nm for the incident polarization and wave propagation direction that are indicated in Figure 2a. The excitation of these dipole and quadrupole resonances produce HSs between the NPs of the dimers that will be analyzed in this work.

The third nanostructure corresponds to a dimer of very irregular NPs (nanopotatoes-like shape)[54] and it is shown in Figure 3. Four different views of this nanostructure (Figure 3a–

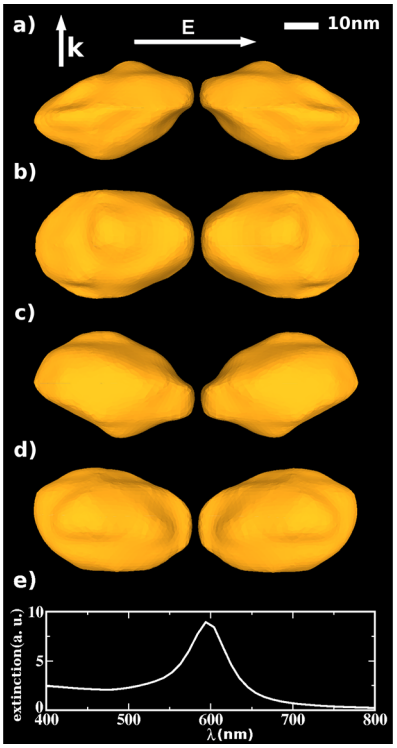

Figure 3. (a–d) Different views of the studied dimer that is formed by irregular Au NPs (nanopotatoes-like shape). The views are obtained by rotating the dimer 90° around its major axis. (e) Extinction spectrum of the dimer for polarization and wave propagation direction which are indicated in Figure 3a.

d) make evident the very irregular shape of the NPs. Equal to the others dimers both NPs are separated by 2 nm but in order to study an HS under completely different conditions respect to the previous nanostructures, the surrounding media and the composition are changed to vacuum and Au, respectively. The extinction spectrum of this dimer is shown in Figure 3e for the incident polarization and wave propagation direction that are indicated in Figure 3a. A HS between the nanopotatoes can be generated at the peak position of the extinction spectrum (λ = 600 nm) that corresponds to a dipole resonance.

The chosen electrodynamic method for the calculations is the discrete dipole approximation (DDA)[55] and the particular conditions of the simulations are displayed in Figures 1a and 2a. Nonlocal[56] or electron confinement effects[57] are not considered

dx.doi.org/10.1021/jp308834e | J. Phys. Chem. C 2013, 117, 7744–7750

in the Ag dielectric constant[58] and a refractive index of n = 1.3330 is used for water.

In the DDA, the object of interest is represented as a cubic array of N polarizable elements. The response of this array to an applied electromagnetic field is described by self-consistently determining the induced dipole moment in each element. This information can be used to determine far-field properties like extinction efficiencies and scattering cross sections.

The near field properties or Γ distributions around NPs were calculated by using probe dipoles.[46] These probe dipoles have a polarizability close to zero in order not to perturb the studied system and they are placed in an extension of the cubic array which is used to represent the NPs in the DDA algorithm. After finishing the DDA calculation successfully, the polarizations of the probes dipoles are obtained. The determination of the electric field in the positions of the probe dipole can be directly obtained by using the following equation

$$\mathbf{E}_j = \alpha_j^{-1}\mathbf{P}_j \tag{1}$$

where α_j is the polarizability tensor and $\mathbf{P}_j$ the calculated polarization of the probe dipole j, whereas $\mathbf{E}_j$ is the electric field on the probe dipole. Finally, Γ is calculated according to

$$\Gamma_j = \frac{\mathbf{E}_j \cdot \mathbf{E}_j^*}{\mathbf{E}_0 \cdot \mathbf{E}_0^*} \tag{2}$$

where $\mathbf{E}_0$ is the incident field.

The concept of VTV[46] consists of determining the variation of the trapped volume between a constant Γ surface and the surface of the NP as a function of the Γ values. From what is explained above, the trapped volume (V_T) is defined as the enclosed volume between a constant Γ surface around a NP and the NP surface boundary.[46] For a given value of Γ, the calculation of V_T can be made by counting (inside the spatial region of the HS) the number of probe dipoles with values of Γ greater than the considered Γ value. A volume of d^3 can be associated to each probe dipole as they are forming a cubic grid with grid size parameter d. A graph of V_T versus Γ for different grid spacing results in a series of curves that are termed as VTV curves.[46] If convergence is reached the trapped volume for a value of enhancement should be invariant upon changing the grid size.[46]

It has been demonstrated that the following expression[46]

$$V_T(\Gamma) = (\Gamma_{V_T=0} - \Gamma)\sum_{i=0}^{2} A_i e^{-\Gamma/k_i} \tag{3}$$

is able to describe quite accurately the converged variation of V_T with Γ for HSs in single NPs. The parameters A_i with unit of volume determine the relative contributions of the different exponential functions whose decays are given by k_i. The root $\Gamma_{V_T=0}$ correspond to the maximum enhancement which is experienced by an unphysical and infinitesimally small object. The above expression makes it evident that there is a gradient of enhancement within an HS. After the parameters of the expression are determined by fitting, the average enhancement ($\bar{\Gamma}$) within a V_T is obtained by using the following equation[46]

$$\bar{\Gamma} = \Gamma_{min} + \frac{1}{V_T(\Gamma_{min})}\int_{\Gamma_{min}}^{\Gamma_{V_T=0}} V_T(\Gamma)\mathrm{d}\Gamma \tag{4}$$

where Γ_{min} is the enhancement for the V_T under consideration. This expression can be reduced to a very simple equation[46]

$$\bar{\Gamma} \approx \Gamma_{min} + k_j \tag{5}$$

if the following conditions are fulfilled

$$\Gamma_{min} \ll \Gamma_{V_T=0} - k_j \quad \text{with} \quad k_j > k_i \wedge j \neq i \tag{6}$$

where k_j is the largest coefficient k_i in eq 3.

A HS is considered as the spatial region with values of Γ greater than the unity.[46] The volume of this region, denoted with Λ,[46] characterizes the degree of localization of an HS and it can be calculated by taking Γ = 1 in eq 3. The mean enhancement within this region, hereinafter denoted by Ξ, can be calculated from eq 4

$$\Xi = 1 + \frac{1}{\Lambda}\int_1^{\Gamma_{V_T=0}} V_T(\Gamma)\mathrm{d}\Gamma \approx 1 + k_j \approx k_j \tag{7}$$

This quantity has been denoted with the Greek letter Ξ in order to remark that Ξ together with Λ are intrinsic quantities of an HS and can be directly obtained from eq 3 just by knowing the greatest coefficient k_i and evaluating V_T for Γ = 1, respectively. It is important to note that to calculate these quantities Λ and Ξ is not trivial and it is easily performed by using the VTV approach.

A new quantity which will be introduced here is the energy which is stored in an HS. This quantity should be helpful to make quantitative correlations among HSs in different nanostructures. From basic physics the instantaneous density of stored energy (μ_e) in a electric field is given by the following equation

$$\mu_e = 1/2\varepsilon_0\varepsilon_r E^2 \tag{8}$$

where ε_0 is the vacuum permittivity, ε_r is the dielectric constant of the surrounding media (ε_r = 1 and ε_r = 1.7689 for vacuum and water, respectively) and E is the electric field. The maximum stored energy in the field of an HS will be given by

$$E_{HS} = 1/2\varepsilon_0\varepsilon_r \int_{V=0}^{V=\Lambda} E^2\,\mathrm{d}V \tag{9}$$

where Λ is by definition the HS volume. Taking into account an incident electric field of E_0 = 1[N/C], this integral can be calculated from

$$\int_{V=0}^{V=\Lambda} E^2\,\mathrm{d}V = \Lambda + \int_{\Gamma=1}^{\Gamma_{V_T=0}} V_T(\Gamma)\mathrm{d}\Gamma = \Xi\Lambda \tag{10}$$

Therefore, the HS energy is given by

$$E_{HS} = 1/2\varepsilon_0\varepsilon_r\Xi\Lambda \tag{11}$$

This is an important result as the energy of an HS can be calculated from Λ and Ξ, which are intrinsic quantities of an HS that are directly obtained from eq 3. Equation 11 also clearly shows the strong relation among Λ and Ξ and E_{HS} and how for a constant value of E_{HS} the enhancement (Ξ) is increased as the degree of localization is increased or, what is the same, as Λ is decreased. This important issue will be addressed in the next section by analyzing the E_{HS} of different nanostructures.

RESULTS AND DISCUSSION

The definition of the V_T for HSs in single NPs, that is, "the enclosed volume between a constant Γ surface around a metal NP and the NP surface boundary",[46] will be also applied here for HSs between two NPs. After applying this definition to the HSs between the two spheres of the dimer, the HSs can be considered as the superposition of two sub-HSs. It means that

dx.doi.org/10.1021/jp308834e | J. Phys. Chem. C 2013, 117, 7744−7750

for high values of Γ there are two constant Γ surfaces that together with the surfaces of the NPs trap or enclose two volumes which are located in different spatial regions.

These regions are very small compared with the dimensions of the HS, and their images from the DDA simulations are poor in quality. Nevertheless, for scholar purposes in Figure 1b is shown in a schematic way the constant Γ surfaces and the trapped volumes expected in this regime. This scheme helps to visualize that HSs between two spheres can be regarded as the superposition of two sub-HSs that each one is located on one sphere.

In the same way, the HSs between the two truncated triangular prism are the superposition of eight sub-HSs that are generated on the vertices of the truncated tips of the NPs (Figure 2b). In general, following the definition of V_T, the HSs between NPs can be considered as the superposition of sub-HSs that are located on the surface of each NP. This fact by itself constitutes a model to describe how the HSs between NPs are generated, and it should be noted that this model arises after applying the definition of the trapped volume to the HS.

As a consequence of the arguments given above, the VTV of HSs between NPs is the sum of the VTV of the different sub-HSs which are located on the NPs surfaces. Equation 3 should describe the VTV of these sub-HSs. For the case of the studied HSs at dipole resonances, the sub-HSs are symmetrical so eq 3 should also describe these HSs. In this way, the VTV approach can be straightforwardly applied also for dimers.

At quadrupole resonance, the sub-HSs cannot be symmetrical as it is the case of the HS between the two triangular prisms where the Γ distribution around NPs depends on the wave vector (**k**) direction. The influence of **k** on the Γ distribution for the studied dimers will be addressed later in the work. Nevertheless, this is not a problem and the HSs can also be analyzed by using the VTV approach.

Figure 4 shows the VTV curves for the HSs between the NPs of the dimers at different values of the grid size parameter *d*. This parameter governs the accuracy of the final computational results of the DDA algorithm. The axes of the graphs have been truncated in order to get a better view of the VTV curves. On panel (a), the VTV curves for the HS that is generated between the NPs of the sphere dimer at dipole resonance (λ = 520 nm) are shown. As it was demonstrated for HSs on single NPs,[46] these curves constitute a method to directly analyze the convergence of Γ calculations. These curves are indicating that the convergence has been reached for $d \approx 0.35$ nm. The VTV curves for the HS at the quadrupolar resonance (λ = 430 nm) are shown in Figure 4b. As for the dipole resonance, the VTV curve for $d \approx 0.35$ nm represents the most reliable variation of V_T with Γ. For the other studied case, that is, the HSs between the truncated triangular prisms, a converged VTV curve is obtained with the same $d \approx 0.4$ nm for the dipole mode (λ = 932 nm) and for the quadrupole mode (λ = 550 nm) as Figure 4c,d, respectively, show.

The four converged VTV curves could be described by eq 3 and the optimization parameters are tabulated in Table 1. The root-mean-square (RMS) percent error and the correlation coefficient indicate the excellent quality of the fitting.

It is important to note that the adjusted expressions to the converged VTV curves describe the sum of the VTV of the sub-HSs that are located on the NP surfaces. In the case of the HSs between the spheres, at very high values of Γ the trapped volume that is obtained from this expression will be distributed in two different spatial regions. These regions are located on each NP surface as Figure 1b schematizes. At lower values of Γ, these two regions will overlap resulting in one region that constitutes the analyzed HS.

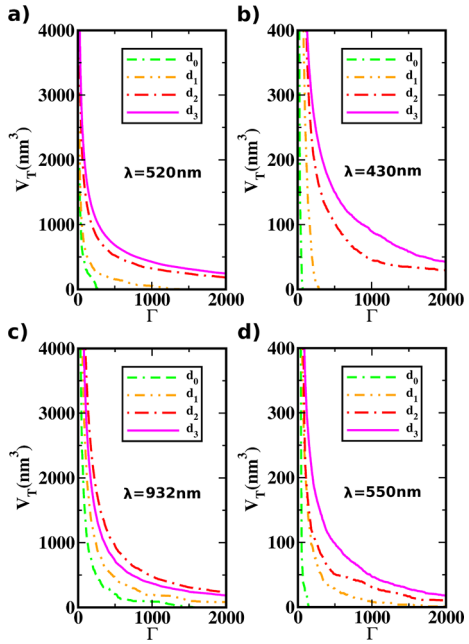

Figure 4. (a) VTV curves for the HS between the spheres at dipole resonance (λ = 520 nm) for different values of grid size parameter d_0 = 1.5 nm, d_1 = 1 nm, d_2 = 0.5 nm, and d_3 = 0.35 nm. (b) VTV curves for the HS between the spheres at quadrupole resonance (λ = 430 nm) for same values of grid size parameter of panel (a). (c) VTV curves of the HS between the truncated triangular prisms at dipole resonance (λ = 932 nm) for different values of grid size parameter d_0 = 1 nm, d_1 = 0.75 nm, d_2 = 0.5 nm, and d_3 = 0.4 nm. (d) VTV curves for the HS between the truncated triangular prisms at quadrupole resonance (λ = 550 nm) for same values of grid size parameter of panel (c).

Table 1. Parameters of the Analytical VTV Expression 3 for Each Analyzed HS in This Work

parameters	dimer of spheres		dimer of triangular prism	
wavelength	λ = 430 nm	λ = 520 nm	λ = 550 nm	λ = 932 nm
$\Gamma_{V_T=0}$	70081	32995	65821	20061
A_0 (nm^3)	0.445	0.151	0.523	0.530
k_0	8.7	32.0	8.5	39.9
A_1 (nm^3)	0.065	0.047	0.030	0.138
k_1	29.5	286.7	37.5	232.7
A_2 (nm^3)	0.0054	0.015	0.004	0.025
k_2	596.6	3420.9	542.4	2361.6
RMS percent error	0.09	0.09	0.07	0.09
correlation coefficient	0.999	0.999	0.999	0.999
$\Gamma_{V_T=0.125\ nm3}$	4741	23907	4115	15917
$\bar{\Gamma}_{V_T=0.125\ nm3}$	5332	26132	4652	17165

For the HSs between the prisms, unlike the case of the sphere dimer, at very high values of enhancement V_T is distributed in eight different spatial regions that are located on the vertices of the truncated extreme of the triangular prisms (Figure 2b). These eight spatial regions overlap at lower values of Γ resulting in a single HS between the NPs.

Figure 5 shows the VTVs that are obtained from the adjusted expressions for the four HSs. Comparing the VTVs at low values of Γ, V_T is higher for the quadrupole resonances than for

dx.doi.org/10.1021/jp308834e | J. Phys. Chem. C 2013, 117, 7744−7750

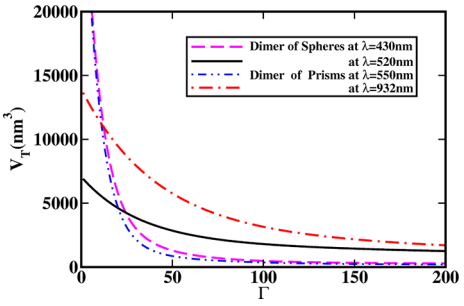

Figure 5. Comparison among the VTVs which are obtained from eq 3 for the studied HSs between the NPs of the sphere dimer and the truncated triangular prism dimer at dipole and quadrupole resonances, as indicated in the inset.

the dipole resonances indicating that the electromagnetic enhancements are more delocalized in the quadrupole mode. On the other hand, the fact that V_T decays faster with Γ for quadrupole resonances than for the dipole ones leads to a lower enhancements inside HSs for the quadrupole mode than for the dipole one. Figure 5 also shows that fields in the HSs at dipole resonances are more confined in the case of the sphere dimer than in the prism dimer case. This can be appreciated by looking V_T when Γ trends to the unity as V_T for the sphere dimer is always smaller than for the prisms dimer at dipole resonance. It is important to note that the VTV is fully characterizing an HS as it shows the field enhancements inside an HS, the spatial regions that are being occupied for such enhancements and also the stored energy in the HS.

Another important aspect to mention is that the VTVs at quadrupole resonances are very similar despite the great morphological differences between the dimers and the different excitation wavelengths. These features are clearly displayed in Figures 6a and 6b that show the Γ distributions around the NPs for the converged simulations.

For Γ > 20, a more extended HS between the NPs is observed for quadrupole resonances (λ = 430 nm and λ = 550 nm) than for dipole modes (λ = 520 nm and λ = 932 nm). This fact is particularly evident between the prisms since at λ = 932 nm values of Γ > 20 are concentrated between the truncated tips while for λ = 550 nm they are spread on the edges of the prisms. For values of Γ > 100 and Γ > 1000, the opposite trend is evident, that is, V_T is greater for the dipole than for the quadrupole mode.

Figure 6a also shows the influence of **k** on the Γ distribution. For λ = 430 nm and Γ > 20, the Γ distribution between the spheres seems to follow the direction of **k**. Despite of this fact both sub-HSs are symmetrical. The influence of **k** is also present in the HSs of the prisms dimer at λ = 550 nm. In this case, **k** is perpendicular to the bases of the prisms and produces a symmetry breaking in the sub-HS that are aligned with the direction of **k**. This effect is observed by a careful analysis at very high values of Γ and it can not be appreciated in Figure 6b.

In order to make a quantitative comparison between the studied HSs, it will be instructive to calculate Γ for a typical volume of V_T = 0.125 nm^3 that can be associated with a dye molecule. By using the analytical VTV expression for each HS, the minimum (Γ) and the mean ($\bar{\Gamma}$) value of Γ inside this volume can be obtained. Table 1 summarizes all of these quantities for the four HSs. An inspection of them indicates that the molecule should experience the highest enhancement inside the HS of the sphere dimer by exciting the dipole mode

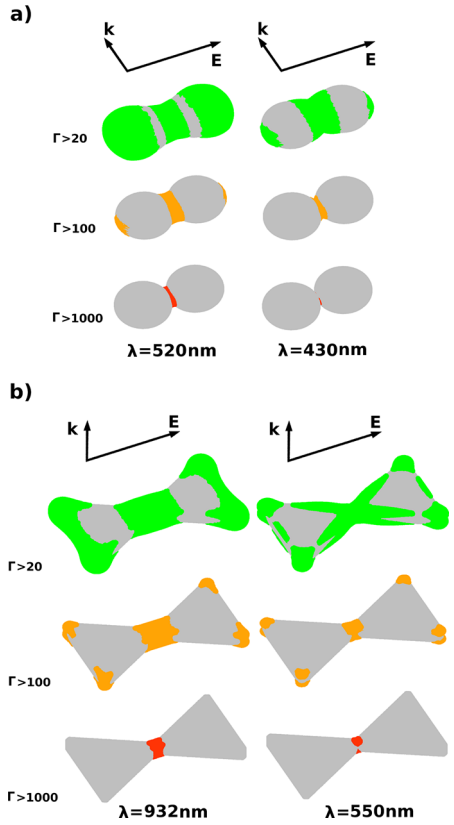

Figure 6. (a) Γ distributions for Γ > 20, Γ > 100, and Γ > 1000 around the sphere dimer. Left: λ = 520 nm. Right: λ = 430 nm. (b) Γ distributions for Γ > 20, Γ > 100, and Γ > 1000 around the prism dimer. Left: λ = 932 nm. Right: λ = 550 nm.

and that the mean value of this enhancement should be $\bar{\Gamma}$ = 26132. It is important to note that the experienced enhancement by the molecule in the HSs at quadrupole resonances (λ = 430 nm and λ = 550 nm) are similar for both types of dimers. This is a consequence of the similarity between the VTVs of both HSs.

In principle, it could be thought that high values of Γ inside an HS should be associated to an HS that is occupying a very small spatial region. However, the value of Γ inside an HS will depend of the energy of an HS. A quantitative way to compare HSs in different nanostructures is by calculating Λ, Ξ, and E_{HS}, quantities that are obtained from the VTV approach. Table 2 shows the values of E_{HS} as well as Ξ and Λ for the analyzed HSs in this work and it also includes values for the same quantities

Table 2. Values of Degree of Localization (Λ), Mean Enhancement (Ξ), and HS Energy (E_{HS}) for the Dimer HSs and for HSs on Single NPs That Have Been Analyzed Before[46]

HS	λ (nm)	Λ (nm^3)	Ξ	E_{HS} (nJ)
dimer of	430	32614	596.6	15.24×10^{-23}
spheres	520	6888	3420.9	18.45×10^{-23}
dimer of	550	32779	542.4	13.92×10^{-23}
prisms	932	13629	2361.6	25.20×10^{-23}
spheroid	432	1909	94.2	0.079×10^{-23}
prism	537	472	401.5	0.084×10^{-23}
cylinder	465	39557	761.6	13.33×10^{-23}

dx.doi.org/10.1021/jp308834e | J. Phys. Chem. C 2013, 117, 7744−7750

for HSs on single NPs (in vacuum) that has been studied before, for comparative purposes.[46]

The values of E_{HS} and Λ clearly indicate that HSs with high energies can produce strong enhancements if this energy is not spread. For example, the HSs in the dimers and the HS on the single cylinder have almost the same energies but the highest value of Γ is obtained in the HS of the sphere dimer at dipolar resonance where this energy is highly confined (Λ = 6888 nm^3).

The confinement of this energy in the HSs of the dimers at quadrupolar resonance and the HS on single cylinder is almost the same (Λ = 32614 nm^3, Λ = 32779 nm^3, and Λ = 39557 nm^3), which gives rise to very similar enhancements inside these HSs. On the other hand, the degree of localization of the HSs on single prism and spheroid is higher (Λ = 472 nm^3 and Λ = 1909 nm^3) but their energies are smaller, therefore the values of Γ inside these HSs are also smaller.

Calculating the E_{HS} in this way, it is possible to make a quantitative comparison between quite different HSs if they have similar E_{HS} values. It is clear from Table 2 that two HSs with similar E_{HS} values, the enhancement is larger for the HS having a lower spread of this energy; that is, a lower Λ value. A speculation arising from the above explanation is that the HSs energy does not seem to depend on the nanoestructure shape but this shape seems to determine the degree of localization. Further work on this issue should be interesting to carry out. In particular, it should be interesting to study the parameters that determine the E_{HS} and Λ values as increasing the energy and degree of localization should also greatly increase the HS performance.

Experimentally, geometric figures are only found in NPs having a relative small number of atoms. In general, wet chemical syntesis give rise to NPs with rounded edges and tips and their shapes are far from being geometric figures.[52−54] In this sense, the HS between two irregular NPs like the nanopotatoes show in Figure 3, constitutes an interesting case to extend and demonstrate the capabilities of the above VTV analysis in a more realistic system. After analyzing this HS by using the VTV approach, values for Λ = 13662 nm^3, Ξ = 1591, and E_{HS} = 9.63 × 10^{-23} nJ are obtained.

By using this values, it is easy to analyze and compare the HS with the previous studied ones. The *Au* nanopotatoes are able to produce an HS with a degree of localization similar to the HS in the prism dimer at dipole resonance but its energy is the lowest among the studied dimers. Therefore, this HS does not produce higher Γ values than the other dimers at dipole resonance. The structure of this HS is formed by two sub-HS because the tips of the nanopotatoes are smooth surfaces as the case of the sphere dimer.

The convergence analysis of Γ calculations for this HS is shown in Figure 7a. This VTV analysis indicates that with a value of $d \approx 0.5$ nm a smooth and appropriate VTV curve is obtained. The parameters of eq 3 for this curve are $\Gamma_{V_T=0}$ = 201 728, A_0 = 0.053, k_0 = 21.664, A_1 = 0.0144, k_1 = 149.547, A_2 = 0.003, and k_2 = 1591.840 with an RMS percent error = 0.076 and correlation coefficient = 0.999. Figure 7b shows the spatial Γ distribution around the dimer for values of Γ > 20, Γ > 100, and Γ > 1000. Note that values of Γ > 1000 are only found between the NPs.

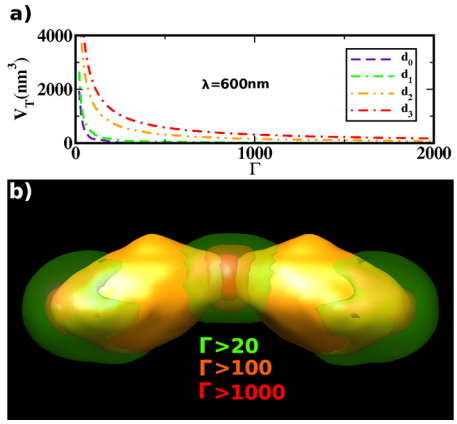

Figure 7. (a) VTV curves for the HS between the nanopotatoes at dipole resonance (λ = 600 nm) for different values of grid size parameter d_0 = 1.5 nm, d_1 = 1 nm, d_2 = 0.75 nm, and d_3 = 0.5 nm. (b) Γ distributions for Γ > 20, Γ > 100, and Γ > 1000 around the dimer.

CONCLUSIONS

To summarize this work, HSs between NPs of three different dimers have been studied by using the VTV approach.

The analysis shows that the HSs between NPs are the superposition of different sub-HSs that are generated on the surface of each NP of the dimer. This result gives a new insight to analyze and understand the plasmonic coupling between NPs and the HSs that are generated from this coupling as well as it enables one to visualize and design plasmonic devices in a better way. For example, in order to modify the features or performance of an HS between two NPs, these sub-HS could be produced in particular locations on the NP surfaces by introducing surface defects.

An important result of this work is that the HSs are almost fully characterized by two quantities that are directly obtained from an expression that describes the VTV of an HS. These quantities are the degree of localization and the mean value of Γ inside the HS. The E_{HS} is calculated from these two quantities and it is equivalent to the area below the VTV curve of an HS. By introducing these quantities it is possible to make a quantitative comparison among HSs of different nanostructures. Provided that two HSs in different nanostructures have the same energy, the present analysis shows that it is necessary to confine this energy to achieve huge values of enhancements inside an HS. In particular, the values of this energy for the studied HSs is almost similar despite the great differences between the nanostructures and the different values of wavelengths that are used to generate the HSs.

The characterization of the HSs shows that a nanostructure with low complexity like a Ag sphere dimer can produce stronger enhancements than a more complex nanostructures as the other analyzed dimer here. The present way of analyzing HSs can be applied to nanostructures of any shape as it has been demonstrated for a highly irregular Au dimer.

AUTHOR INFORMATION

Corresponding Author

*E-mail: coronado@fcq.unc.edu.ar.

Notes

The authors declare no competing financial interest.

dx.doi.org/10.1021/jp308834e | *J. Phys. Chem. C* 2013, 117, 7744−7750

■ ACKNOWLEDGMENTS

The authors thanks CONICET, Fundación Antorchas, SECYT-UNC, and FONCYT for financial support.

■ REFERENCES

(1) Halas, N. J.; Lal, S.; Chang, W.-S.; Link, S.; Nordlander, P. *Chem. Rev.* **2011**, *111* (6), 3913−3961.
(2) Bek, A.; Jansen, R.; Ringler, M.; Mayilo, S.; Klar, T. A.; Feldmann, J. *Nano Lett.* **2008**, *8*, 485−490.
(3) Perassi, E. M.; Scarpettini, A. F.; Masip, M. E.; Bragas, A. V.; Coronado, E. A. *J. Phys. Chem. C* **2011**, *115* (21), 10455−10461.
(4) Hao, E.; Schatz, G. C. *J. Chem. Phys.* **2004**, *120*, 357−366.
(5) Foteinopoulou, S.; Vigneron, J. P.; Vandenbem, C. *Opt. Express* **2007**, *15*, 4253−4267.
(6) Stiles, P. L.; Dieringer, J. A.; Shah, N. C.; Duyne, R. P. V. *Annu. Rev. Anal. Chem.* **2008**, *1*, 601−26.
(7) Lee, S. J.; Guan, Z.; Xu, H.; Moskovits, M. *J. Phys. Chem. C* **2007**, *111* (49), 17985−17988.
(8) Le, F.; Brandl, D. W.; Urzhumov, Y. A.; Wang, H.; Kundu, J.; Naomi J. Halas, J. A.; Nordlander, P. *ACS Nano* **2008**, *2* (4), 707−718.
(9) Haynes, C. L.; Duyne, R. P. V. *J. Phys. Chem. B* **2003**, *107*, 7426−7433.
(10) Dieringer, J. A.; McFarland, A. D.; Shah, N. C.; Stuart, D. A.; Whitney, A. V.; Yonzon, C. R.; Young, M. A.; Zhang, X.; Duyne, R. P. V. *Faraday Discuss.* **2006**, *132*, 9−26.
(11) Metiu, H. *Prog. Surf. Sci.* **1984**, *17* (3−4), 153−320.
(12) Ru, E. C. L.; Etchegoin, P. G. *Principles of Surface-Enhanced Raman Spectroscopy*; Elsevier: New York, 2008.
(13) Nie, S.; Emory, S. R. *Science* **1997**, *275*, 1102−1106.
(14) Kneipp, K.; Wang, Y.; Kneipp, H.; Perelman, L. T.; Itzkan, I.; Dasari, R. R.; Feld, M. S. *Phys. Rev. Lett.* **1997**, *78*, 1667−1670.
(15) Dieringer, J. A.; Wustholz, K. L.; Masiello, D. J.; Camden, J. P.; Kleinman, S. L.; Schatz, G. C.; Duyne, R. P. V. *J. Am. Chem. Soc.* **2009**, *131* (2), 849−854.
(16) Kleinman, S. L.; Ringe, E.; Valley, N.; Wustholz, K. L.; Phillips, E.; Scheidt, K. A.; Schatz, G. C.; Duyne, R. P. V. *J. Am. Chem. Soc.* **2011**, *133* (2), 4115−4122.
(17) Xu, H.; Bjerneld, E. J.; Börjesson, M. K. L. *Phys. Rev. Lett.* **1999**, *83* (21), 4357−4360.
(18) Michaels, A. M.; Nirmal, M.; Brus, L. E. *J. Am. Chem. Soc.* **1999**, *121* (43), 9932−9939.
(19) Xu, H.; Aizpurua, J.; Käll, M.; Apell, P. *Phys. Rev. E* **2000**, *62* (3), 4318−4324.
(20) Zhang, W.; Cui, X.; Yeo, B.-S.; Schmid, T.; Hafner, C.; Zenobi, R. *Nano Lett.* **2008**, *7* (5), 1401−1405.
(21) Becker, M.; Sivakov, V.; Andrä, G.; Geiger, R.; Schreiber, J.; Hoffmann, S.; Michler, J.; Milenin, A. P.; Werner, P.; Christiansen, S. H. *Nano Lett.* **2007**, *7* (1), 75−80.
(22) Pettinger, B. *Top. Appl. Phys* **2006**, *103*, 217.
(23) Stöckle, R. M.; Suh, Y. D.; Deckert, V.; Zenobi, R. *Chem. Phys. Lett.* **2000**, *318*, 131−136.
(24) Hayazawa, N.; Tarun, A.; Inouye, Y.; Kawata, S. *J. Appl. Phys.* **2002**, *92* (12), 6983−6986.
(25) Hartschuh, A.; Beversluis, M. R.; Bouhelier, A.; Novotny, L. *Philos. Trans. R. Soc. London, Ser. A* **2004**, *362*, 807−819.
(26) Bailo, E.; Deckert, V. *Chem. Soc. Rev.* **2008**, *37*, 921−930.
(27) Pettinger, B.; Domke, K. F.; Zhang, D.; Picardi, G.; Schuster, R. *Surf. Sci.* **2009**, *603*, 1335−1341.
(28) Tarun, A.; Hayazawa, N.; Kawata, S. *Anal. Bioanal. Chem.* **2009**, *394*, 1775−1785.
(29) Li, J. F.; Huang, Y. F.; Ding, Y.; Yang, Z. L.; Li, S. B.; Zhou, X. S.; Fan, F. R.; Zhang, W.; Zhou, Z. Y.; Wu, D. Y.; Ren, B.; Wang, Z. L.; Tian, Z. Q. *Nature* **2010**, *464* (7287), 392−395.
(30) Kinkhabwala, A.; Yu, Z.; Fan, S.; Avlasevich, Y.; Moerner, K. M. W. E. *Nat. Photonics* **2009**, *3*, 654−657.
(31) Stranik, O.; Nooney, R.; McDonagh, C.; MacCraith, B. D. *Plasmonics* **2007**, *2*, 15−22.
(32) Girard, C.; Martin, O. J. F.; Dereux, A. *Phys. Rev. Lett.* **1995**, *75*, 3098−3101.
(33) Chowdhury, M. H.; Ray, K.; Aslan, K.; Lakowicz, J. R.; Geddes, C. D. *J. Phys. Chem. C* **2007**, *111*, 18856−18863.
(34) Yang, X.; Gu, C.; Qian, F.; Li, Y.; Zhang, J. Z. *Anal. Chem.* **2011**, *83*, 5888−5894.
(35) Srituravanich, W.; Fang, N.; Sun, C.; Luo, Q.; Zhang, X. *Nano Lett.* **2004**, *4* (6), 1085−1088.
(36) Sundaramurthy, A. *Nano Lett.* **2006**, *6*, 355−360.
(37) Ozbay, E. *Science* **2006**, *311*, 189−193.
(38) Atwater, H. *Sci. Am.* **2007**, *296*, 56−63.
(39) Frey, H. G.; Witt, S.; Felderer, K.; Guckenberger, R. *Phys. Rev. Lett.* **2004**, *93*, 200801.
(40) Novotny, L.; Stranick, S. J. *Annu. Rev. Phys. Chem.* **2006**, *57*, 303−31.
(41) Angelis, F. D.; Patrini, M.; Das, G.; Maksymov, I.; Galli, M.; Businaro, L.; Andreani, L. C.; Fabrizio, E. D. *Nano Lett.* **2008**, *8* (8), 2321−2327.
(42) Anker, J. N.; Hall, W. P.; Lyandres, O.; Shah, N. C.; Zhao, J.; Duyne, R. P. V. *Nat. Mater.* **2008**, *7*, 442−453.
(43) Georganopoulou, D. G.; Chang, L.; Nam, J.-M.; Thaxton, C. S.; Mufson, E. J.; Klein, W. L.; Mirkin, C. A. *Proc. Natl Acad. Sci. U.S.A.* **2005**, *107*, 2273−2276.
(44) Haes, A. J.; Chang, L.; Klein, W. L.; Duyne, V. R. P. *J. Am. Chem. Soc.* **2005**, *127*, 2264−2271.
(45) Sherry, L. J.; Jin, R.; Mirkin, C. A.; Schatz, G. C.; Duyne, R. P. V. *Nano Lett.* **2006**, *6* (9), 2060−2065.
(46) Perassi, E. M.; Canali, L. R.; Coronado, E. A. *J. Phys. Chem. C* **2009**, *113* (16), 6315−6319.
(47) Fischer, H.; Martin, O. J. F. *Opt. Express* **2008**, *16*, 9144−9154.
(48) Li, W.; Camargo, P. H. C.; Lu, X.; Xia, Y. *Nano Lett.* **2009**, *9*, 485−490.
(49) Lin, H.-Y.; Huang, C.-H.; Chang, C.-H.; Lan, Y.-C.; Chui, H.-C. *Opt. Express* **2010**, *18*, 165−172.
(50) Schuck, P. J.; Fromm, D. P.; Sundaramurthy, A.; Kino, G. S.; Moerner, W. E. *Phys. Rev. Lett.* **2005**, *94*, 017402.
(51) Kinkhabwala, A.; Yu, Z.; Fan, S.; Avlasevich, Y.; Mullen, K.; MoernerW., E. *Nat. Photonics* **2009**, *3*, 654−657.
(52) Perassi, E. M.; Hernandez-Garrido, J. C.; Moreno, M. S.; Encina, E. R.; Coronado, E. A.; Midgley, P. A. *Nano Lett.* **2010**, *10*, 2097−2104.
(53) Leary, R.; Midgley, P. A.; Thomas, J. M. *Acc. Chem. Res.* **2012**, *45*, 1782−1791.
(54) Kern, A. M.; Martin, O. J. F. *Nano Lett.* **2011**, *11*, 482−487.
(55) Purcell, E. M.; Pennypacker, C. R. *Astrophys. J.* **1973**, *186*, 705−714.
(56) McMahon, J. M.; Gray, S. K.; Schatz, G. C. *Phys. Rev. Lett.* **2009**, *103* (9), 097403.
(57) Coronado, E. A.; Schatz, G. C. *J. Chem. Phys.* **2003**, *119*, 3926.
(58) Palik, E. D. *Handbook of Optical Constant of Solids*; Academic Press: New York, 1985.